The Plant Cell, Vol. 31: 848–861, April 2019, www.plantcell.org © 2019 ASPB.

PRX9 and PRX40 Are Extensin Peroxidases Essential for Maintaining Tapetum and Microspore Cell Wall Integrity during Arabidopsis Anther Development

Joseph R. Jacobowitz,[a,b] William C. Doyle,[a] and Jing-Ke Weng[a,b,1]

[a] Whitehead Institute for Biomedical Research, Cambridge, Massachusetts 02142
[b] Department of Biology, Massachusetts Institute of Technology, Cambridge, Massachusetts, 02139

ORCID IDs: 0000-0001-6289-8889 (J.R.J.); 0000-0002-2777-8037 (W.C.D.); 0000-0003-3059-0075 (J.-K.W.)

Pollen and microspore development are essential steps in the life cycle of all land plants that generate male gametes. Within flowering plants, pollen development occurs inside of the anther. Here, we report the identification of two class III peroxidase-encoding genes, *PEROXIDASE9* (*PRX9*) and *PRX40*, that are genetically redundant and essential for proper anther and pollen development in Arabidopsis (*Arabidopsis thaliana*). Arabidopsis double mutants devoid of functional *PRX9* and *PRX40* are male sterile. The mutant anthers display swollen, hypertrophic tapetal cells and pollen grains, suggesting disrupted cell wall integrity. These phenotypes lead to nearly 100%-penetrant pollen degeneration upon anther maturation. Using immunochemical and biochemical approaches, we show that PRX9 and PRX40 likely cross-link extensins to contribute to tapetal cell wall integrity during anther development. This work suggests that *PRX9* and *PRX40* encode Arabidopsis extensin peroxidases and highlights the importance of extensin cross-linking during pollen development.

INTRODUCTION

Pollen performs a critical step in the flowering plant life cycle by transporting the male gamete to the female ovule for fertilization. To do this, pollen must survive the journey from its origin in the anther to its destination atop the carpel. Wind-borne or insect-dispersed pollen may need to travel great distances to reach a suitable carpel. During its journey, pollen must endure a wide range of abiotic stresses, including UV radiation, extreme temperatures, and desiccation. To survive these challenges, pollen grains are protected by a unique and specialized cell wall.

The synthesis of the pollen wall was one of the most important innovations that enabled plant life on land. The pollen wall is highly structured and indispensable for pollen vitality. It is composed of two parts: an outer exine and an inner intine (Heslop-Harrison, 1968). The exine is composed of a uniquely robust polymer called sporopollenin. Many genes involved in the biosynthesis of sporopollenin have been identified, mostly through genetic studies, but the detailed chemical structure of the polymer is poorly understood (Quilichini et al., 2015). The intine resembles a conventional plant cell wall and consists of cellulose, hemicellulose, and pectin as well as cell wall–associated proteins (Knox et al., 1970). Pollen development occurs in the anther, concurrent with anther development.

Arabidopsis (*Arabidopsis thaliana*) anthers are specialized organs that are designed to produce and release pollen grains. Arabidopsis flowers have six anthers that are positioned atop anther filaments and encircle the female carpel. Each anther has four functionally equivalent lobes. Within each lobe, pollen develops in a chamber known as the locule. Locule walls are lined by a specialized tissue composed of secretory cells known as the tapetum. The tapetum is the innermost layer of the anther and provides nutrients to developing pollen grains. The tapetum is also thought to supply the sporopollenin precursors that later polymerize to form the pollen exine. At late stages of pollen development, the tapetum undergoes programmed cell death (PCD), depositing a mixture of protein and wax on the surface of the exine, known as tryphine (Heslop-Harrison, 1968).

Although the sequence of events in tapetum and pollen development has been well described, the exact biochemical processes involved remain poorly understood. In the model plant Arabidopsis, hundreds of evolutionarily conserved genes are specifically expressed in developing anthers, but only a few have been functionally characterized to date (Li et al., 2017). In this work, we sought to better understand the role of a subset of these genes encoding class III peroxidases.

Class III peroxidases are a large family of heme-iron–dependent peroxidases that arose specifically within land plants and have expanded widely since their emergence; the Arabidopsis genome contains 73 members (Tognolli et al., 2002; Welinder et al., 2002; Duroux and Welinder, 2003; Weng and Chapple, 2010). Many biochemical activities important for various aspects of land plant physiology have been attributed to class III peroxidases. For example, class III peroxidases oxidatively polymerize monolignols in the apoplast of the lignifying cells. Previous studies have found that *PEROXIDASE2* (*PRX2*), *PRX4*, *PRX17*, *PRX25*, *PRX52*, *PRX71*, and *PRX72* are involved in stem lignification in Arabidopsis (Herrero et al., 2013; Fernández-Pérez et al., 2015a, 2015b; Shigeto et al., 2015). In addition, class III peroxidases are also thought to polymerize other elements of the plant cell wall, including suberin and extensins (Bernards et al., 1999; Jackson

[1] Address correspondence to wengj@wi.mit.edu.
The author responsible for distribution of materials integral to the findings presented in this article in accordance with the policy described in the Instructions for Authors (www.plantcell.org) is: Jing-Ke Weng (wengj@wi.mit.edu).
www.plantcell.org/cgi/doi/10.1105/tpc.18.00907

IN A NUTSHELL

Background: Just like all organisms, plants must reproduce for the continued survival of their species. Moreover, humans are directly dependent on plant reproduction for food, oil, fiber, and more. Most plants that we encounter in day-to-day life reproduce by making pollen. When pollen grains aren't irritating our sinuses, they are serving as protective capsules that transport precious cargo. Inside the tough walls of pollen grains are the male gamete cells that will fertilize the female ovules. This process of fertilization produces the seed, and subsequently the next generation. Therefore, it's critical that a plant succeed in producing pollen. Pollen production occurs in the anthers, which are structures that are typically seen on top of stems in the interiors of flowers. Although we know a lot about anthers, there are still many genes that are important for anther development that we don't fully understand.

Question: Here, we built upon previous works that compiled extensive datasets detailing gene expression in anthers. We focused on an important family of plant enzymes: Class III peroxidases. We sought to understand if any Class III peroxidases are important for anther and pollen development. If so, what do they do?

Findings: We discovered two enzymes, PEROXIDASE9 and PEROXIDASE40, which are essential for anther development. When these genes are disrupted *Arabidopsis thaliana* cannot make pollen. Without these peroxidases, a special set of cells in the anther swells and the pollen grains degenerate. These swollen cells are known as tapetal cells and they form the walls of the chamber in which pollen develops. We demonstrate that these peroxidases likely reinforce tapetal cell walls by cross-linking structural extensin proteins. The lack of cross-linking results in a compromised cell wall, which cannot withstand turgor pressure, leading to swelling.

Next steps: Arabidopsis has 73 different Class III peroxidases and 20 different extensin proteins. We only know the functions for a fraction of these genes. In this work, we uncovered a role for two peroxidases in the anther. Future work will likely continue to dissect the different contributions that Class III peroxidases and extensins make towards plant development and fitness.

et al., 2001). Conversely, some class III peroxidases may function to destabilize plant cell walls by generating hydroxyl radicals that cleave load-bearing cell wall polysaccharides (Liszkay et al., 2004). This is exemplified by *PRX36*, which serves as a seed mucilage extrusion factor by loosening the walls of epidermal cells in the Arabidopsis seed coat (Kunieda et al., 2013).

In this work, we identified two class III peroxidase-encoding genes, *PRX9* and *PRX40*, that are required for proper development of tapetum and microspores in Arabidopsis. The *prx9 prx40* double mutants exhibit distinctive tapetum swelling and enlarged developing pollen grains, ultimately leading to microspore degeneration and male sterility. We provide further evidence that *PRX9* and *PRX40* ensure proper establishment of the tapetum and microspore cell walls by cross-linking extensins.

RESULTS

PRX9 and *PRX40* Are Specifically Expressed in the Tapetum of Developing Anthers

To identify uncharacterized metabolic enzymes involved in pollen and anther development, we performed a coexpression analysis using the known exine biosynthetic genes as search queries (Obayashi et al., 2007). This analysis uncovered only two class III peroxidase genes, *PRX9* (AT1G44970) and *PRX40* (AT4G16270), which are specifically expressed in early stages of flower development (Supplemental Figure 1; Winter et al., 2007; Waese and Provart, 2017). Neither *PRX9* nor *PRX40* has been the focus of any prior publication, but both genes have been implicated in root elongation and lateral root primordia formation (Tsukagoshi et al., 2010; Fernández-Marcos et al., 2017). Nevertheless, *PRX9* and *PRX40* have not been shown to have roles in flower development.

To experimentally examine the tissue specificity of *PRX9* and *PRX40* expression, we first profiled the transcript abundance of *PRX9* and *PRX40* across six different Arabidopsis tissue types by RT-PCR. This experiment verified that *PRX9* and *PRX40* are both specifically expressed in the flower buds, but not in the other five tissues examined (Figure 1A). To obtain higher spatial and temporal resolution for *PRX9* and *PRX40* expression, we generated promoter-β-glucuronidase (GUS) reporter lines for *PRX9* and *PRX40* and examined the tissue-specific GUS activities in six independent T1 transformants for each reporter construct. In both cases, all six replicates produced nearly identical results. Whereas *PRX9* promoter-reporter activity was detected in both early-developing anthers and mature carpels, *PRX40* promoter-reporter activity was exclusively observed in early-developing anthers (Figures 1B to 1D). Closer examination of the GUS-stained anther sections further established that *PRX9* and *PRX40* are specifically expressed in the tapetum (Figure 1E). Expression of *PRX9* and *PRX40* appeared to initiate at anther stage 6 and peak around anther stage 10. No staining was observed in later stages of anther development in which the tapetum had undergone PCD.

PRX9 and PRX40 Are Genetically Redundant and Required for Male Fertility

To probe the in vivo function of *PRX9* and *PRX40*, we obtained two independent T-DNA insertion lines for each of the two genes. SALK_204557 (*prx9-1*) and SAIL_875_A09 (*prx9-2*) contain insertions in the second and fourth exons of *PRX9*, respectively, and SALK_031680 (*prx40-1*) and SALK_061827 (*prx40-2*) contain insertions in the second and first introns of *PRX40*, respectively

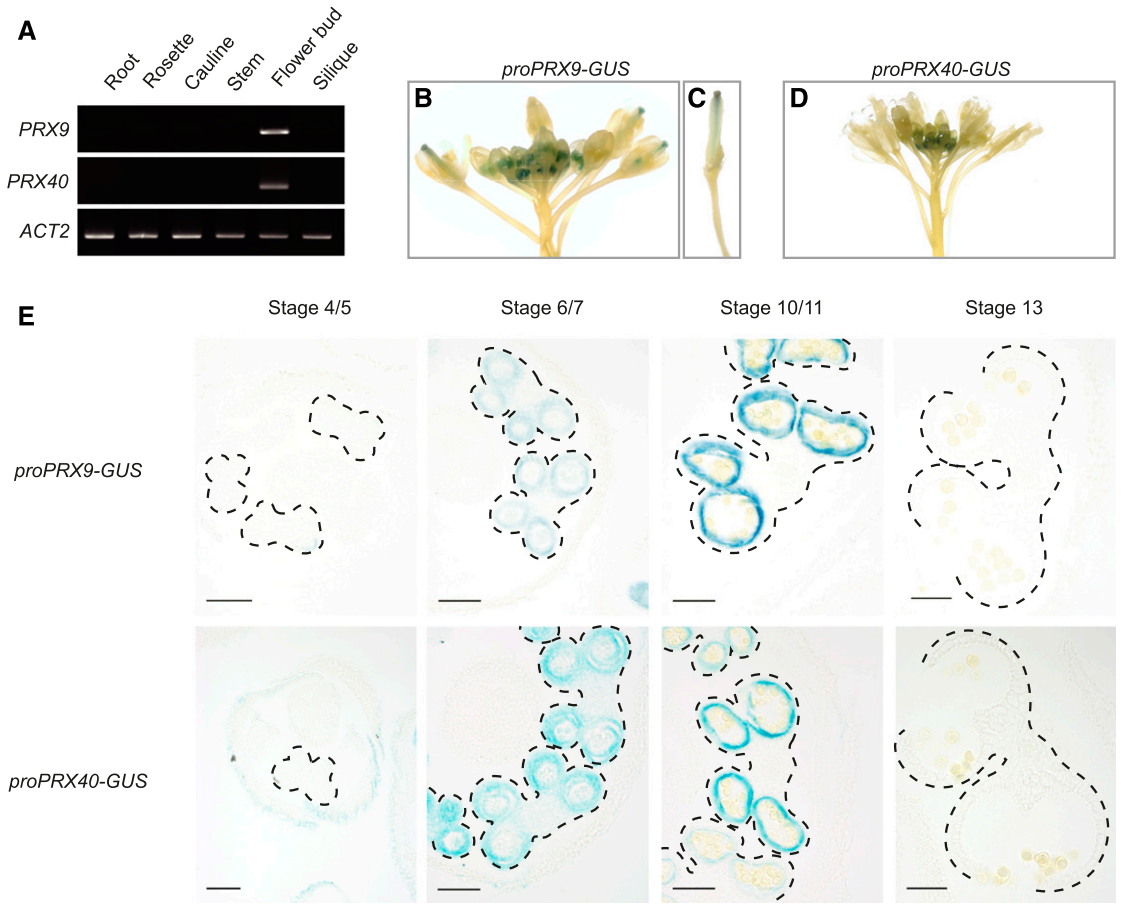

Figure 1. *PRX9* and *PRX40* Are Expressed in the Tapetum of Developing Anthers.

(A) to **(E)** RT-PCR across a variety of Col-0 tissues shows *PRX9* and *PRX40* are specifically expressed in the flower buds **(A)**. The *ACT2* transcript was used as a positive control and could be amplified in all samples. Whole-mount images show reporter *ProPRX9-GUS* activity is detected in the early anthers **(B)** and mature carpel **(C)**. *ProPRX40-GUS* reporter activity is detected in the early anthers **(D)**. Images of anther sections of GUS reporter across development shows that *PRX9* and *PRX40* promoter activity is localized to the tapetum, is initiated by stage 6, and peaks around stage 10 **(E)**. Promoter reporter activity is absent by anther dehiscence. Anthers are outlined with dashed lines. Bars = 50 μm.

(Figure 2A). To assess whether these insertion events resulted in loss-of-function mutations, we examined the expression of *PRX9* and *PRX40* in the T-DNA lines by RT-PCR (Figure 2B) and established that all the four T-DNA insertion events produced loss-of-function alleles.

Single mutants of either *prx9* or *prx40* display no visible differences from the Columbia (Col-0) wild-type plants. In particular, the *prx9* and *prx40* mutants are fully fertile and develop fully elongated, seed-bearing siliques (Figures 3A to 3E).

Since none of the single mutants exhibited any visible phenotype, we hypothesized that *PRX9* and *PRX40* may be genetically redundant. To test this, we generated all four possible *prx9 prx40* double mutants using the four single mutant alleles. In contrast to the single mutants, which displayed no obvious defects in fertility, all *prx9 prx40* double mutant plants were completely sterile (Figures 3F to 3K). Siliques from double mutants were short and contained no seeds. The *prx9 prx40* plants are likely male sterile as *prx9 prx40* plants were readily fertilized by the wild-type pollen, but all attempts to fertilize the wild-type plants with *prx9 prx40* pollen failed. Since two independent alleles are represented for each peroxidase gene, and all four double mutants displayed identical phenotypes, we conclude that *PRX9* and *PRX40* are genetically redundant and required for male fertility in Arabidopsis.

We then examined the flowers from the double mutant at various developmental stages by light microscopy. At stage 14 of anther development (Sanders et al., 1999), the wild-type anthers were coated with mature pollen grains, whereas *prx9-1 prx40-2* anthers were devoid of pollen (Figures 3N and 3O). We also observed that anthers from the *prx9-1 prx40-2* plants displayed defects in anther filament elongation (Supplemental Figure 2). However, this did not appear to be the primary cause of sterility, as *prx9 prx40* anthers were incapable of depositing pollen on the stigma, even when manually crossed. Similar defects in anther filament extension have been previously observed in mutants of other important tapetal regulators, such as *DYSFUNCTIONAL TAPETUM1*, *DEFECTIVE IN TAPETAL DEVELOPMENT AND FUNCTION1*, and *ABORTED MICROSPORES* (Sorensen et al., 2003; Zhang et al., 2006; Zhu et al., 2008). This is likely a secondary effect of tapetal dysfunction that is caused by an impairment of auxin production,

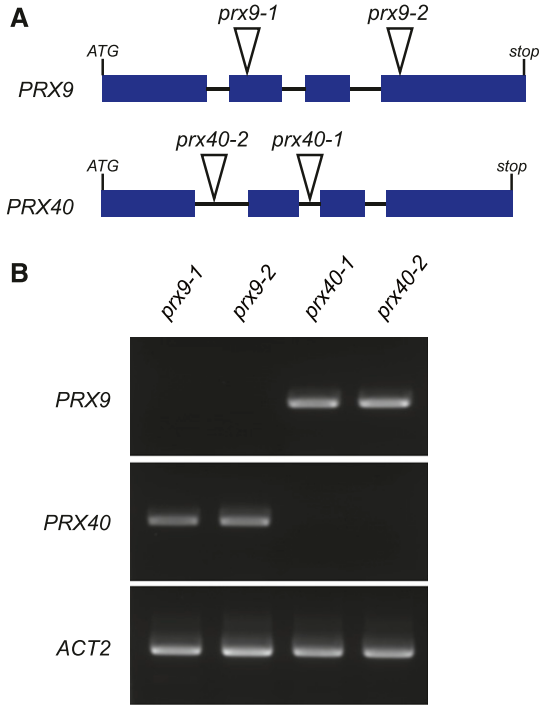

Figure 2. Molecular Characterization of *PRX9* and *PRX40* Insertion Lines.

(A) *prx9-1* and *prx9-2* contain T-DNA insertions in the second and fourth exons of *PRX9*, respectively. *prx40-1* and *prx40-2* contain T-DNA insertions in the second and first introns of *PRX40*, respectively. Blue rectangles represent exons, lines represent introns, and triangles indicate T-DNA insertion sites.

(B) RT-PCR showing full-length *PRX9* cDNA could not be amplified from *prx9-1* or *prx9-2* mutants, while full-length *PRX40* cDNA could not be amplified from *prx40-1* or *prx40-2* mutants. The *ACT2* transcript was used as a positive control and could be amplified in all four samples.

which occurs in the tapetum during anther development (Cecchetti et al., 2008). Since indehiscence is one of the mechanisms that can lead to male sterility even when pollen grains are properly developed (Sanders et al., 1999; Hao et al., 2014; Yang et al., 2017), we examined stage 13 anthers (Sanders et al., 1999; Hao et al., 2014; Yang et al., 2017) by scanning electron microscopy. Anthers from both the wild-type and the *prx9-1 prx40-2* plants clearly showed breakage along the stomiums, indicating that the male-sterility phenotype of *prx9-1 prx40-2* is unlikely to be caused by indehiscence (Figures 3L and 3M).

PRX9 and *PRX40* Play Important Roles in Maintaining Tapetum and Microspore Cell Wall Integrity

To identify the stage at which *prx9-1 prx40-2* anther and pollen development first derails, we performed a histological comparison between the *prx9-1 prx40-2* and the wild-type anthers over various developmental stages (Figure 4). At stages 5 and 6, *prx9-1 prx40-2* and wild-type anthers were indistinguishable. Noticeable differences first appeared at stages 8 and 9, with the double mutant exhibiting ectopically swollen tapetal cells that invade into the locular space. The swollen tapetum persisted through stage 10 in *prx9-1 prx40-2* plants. By stages 11 and 12, the tapetum had degenerated in both plants, but the pollen grains were shriveled and crushed in the *prx9-1 prx40-2* anthers. The appearance of the tapetum swelling phenotype between stages 7 and 10 closely parallels *PRX9* and *PRX40* expression (Figure 1). These observations suggest that the male sterility of *prx9-1 prx40-2* plants is likely caused by tapetum swelling (i.e., tapetum hypertrophy) and subsequent pollen degeneration.

To further characterize the tapetum hypertrophy phenotype, we examined stage 9 anthers by transmission electron microscopy (Figure 5). Consistently, the *prx9-1 prx40-2* sample displayed expanded tapetum cells with enlarged tapetal vacuoles, compared with the wild type. Microspores in *prx9-1 prx40-2* anthers were also abnormally enlarged and vacuolated. The boundaries between tapetal cells in *prx9-1 prx40-2* plants were jigsaw shaped, with one cell swelling into the neighboring cell, whereas the boundaries between tapetal cells in the wild-type plants were typically well defined and straight. This phenotype may be a manifestation of compromised tapetal cell wall integrity. Moreover, we observed aberrant distributions of electron-dense material in the swollen tapetum of *prx9-1 prx40-2* anthers, reminiscent of sporopollenin typically observed at the outer wall of normally developed pollen. By stage 9, the wild-type microspores exhibit a fully developed exine. By contrast, only nexine and probaculae had formed on the microspore surface in the double mutant, with the majority of the sporopollenin-like material accumulated at the locular face of the tapetum. Finally, the middle layer was not crushed in *prx9-1 prx40-2* plants. Taken together, this suggests that PRX9 and PRX40 play an important role in maintaining tapetal and microspore cell size and shape by modulating the cell wall.

PRX9 and PRX40 Are Active Peroxidases In Vitro

To probe the biochemical function of PRX9 and PRX40, we first tested whether PRX9 and PRX40 are catalytically active hydrogen peroxide (H_2O_2)–dependent peroxidases by heterologously expressing PRX9 and PRX40 in *Escherichia coli*. Although both proteins were highly expressed in *E. coli*, they were insoluble. We solubilized recombinant PRX9 and PRX40 by denaturing them in 8 M urea. After purification, we subjected the unfolded PRX9 and PRX40 to a peroxidase refolding screen using pyrogallol as a generic peroxidase substrate (Smith et al., 1990). Refolding conditions were tested for activity by the addition of pyrogallol and H_2O_2. Activity was observed by a colorimetric change associated with an increase in absorbance at 420 nm as pyrogallol was converted into purpurogallin. We optimized the refolding conditions for both PRX9 and PRX40 and observed H_2O_2-dependent peroxidase activity on pyrogallol for both enzymes (Supplemental Figure 3). This result demonstrates that PRX9 and PRX40 behave as typical class III peroxidases and are capable of completing the catalytic cycle in vitro.

PRX9 and *PRX40* Are Likely Extensin Cross-Linking Peroxidases

Since the cell wall exerts a strong influence on the size and shape of plant cells, and since class III peroxidases are typically localized in the plant apoplast, we hypothesized that PRX9 and PRX40 may

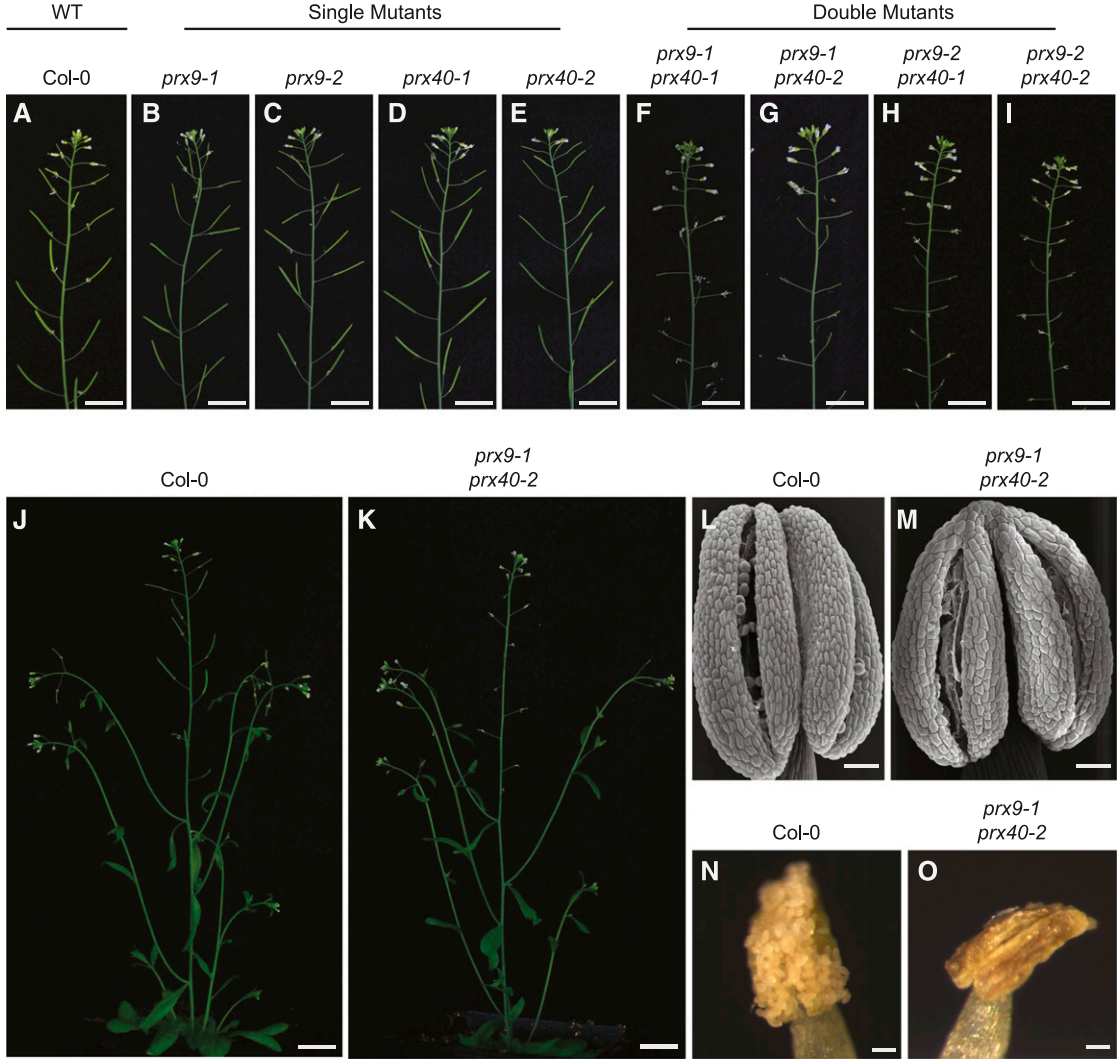

Figure 3. *prx9 prx40* Double Mutants Are Male Sterile and Do Not Produce Viable Pollen.

(A) to **(O)** While the wild-type **(A)** and **(J)**, single *prx9* **(B)** and **(C)**, and single *prx40* **(D)** and **(E)** plants show no defects in fertility, all *prx9 prx40* double mutants **(F)** to **(I)** and **(K)** are male sterile. Bars = 2 cm. Stage 13 wild-type **(L)** and *prx9-1 prx40-2* **(M)** anthers dehisce normally. Bars = 50 μm. Stage 14 wild-type **(N)** anthers are coated in pollen grains. *prx9-1 prx40-2* **(O)** anthers are devoid of pollen grains. Stages according to Sanders et al. (1999). Bars = 50 μm. WT, wild type.

oxidize a component of the tapetum and microspore cell walls and thus reinforce them. Since the tapetum is not thought to be lignified or suberized, extensins stood out as a potential substrate for PRX9 and PRX40. Extensins are structural Hyp-rich glycoproteins in the cell wall that are known to regulate cell size and shape. They form large fibrillar networks and are thought to scaffold the assembly of the plant cell wall (Cannon et al., 2008). Previous studies showed that extensins may be intra- and intermolecularly cross-linked by class III peroxidases via Tyr residues (Fry, 1982; Brownleader et al., 1995, 2000 ; Brady et al., 1996). It is unclear why extensins must be cross-linked, but cross-linking is necessary for their function (Hall and Cannon, 2002; Ringli, 2010).

To assess the role of extensins in tapetal cell development, we first examined the accumulation of extensins in the wild-type anthers by immunostaining. We took advantage of John Innes Monoclonal Antibody 20 (JIM20), a well-characterized extensin-specific monoclonal antibody (Pattathil et al., 2010). Consistent with our hypothesis, JIM20 extensin epitopes were highly enriched in the wild-type tapetum (Figures 6A and 6B). Pollen walls also appeared to be stained, but it is difficult to determine the extent of staining because pollen grains are naturally pigmented.

Since cross-linking increases the apparent molecular weight of extensins, we expected high molecular weight extensins to accumulate in the tapetum of the wild-type anthers. If PRX9 and PRX40 were the primary extensin peroxidases in tapetum, we would expect *prx9-1 prx40-2* anthers to accumulate less high molecular weight extensins. To test this hypothesis, we performed

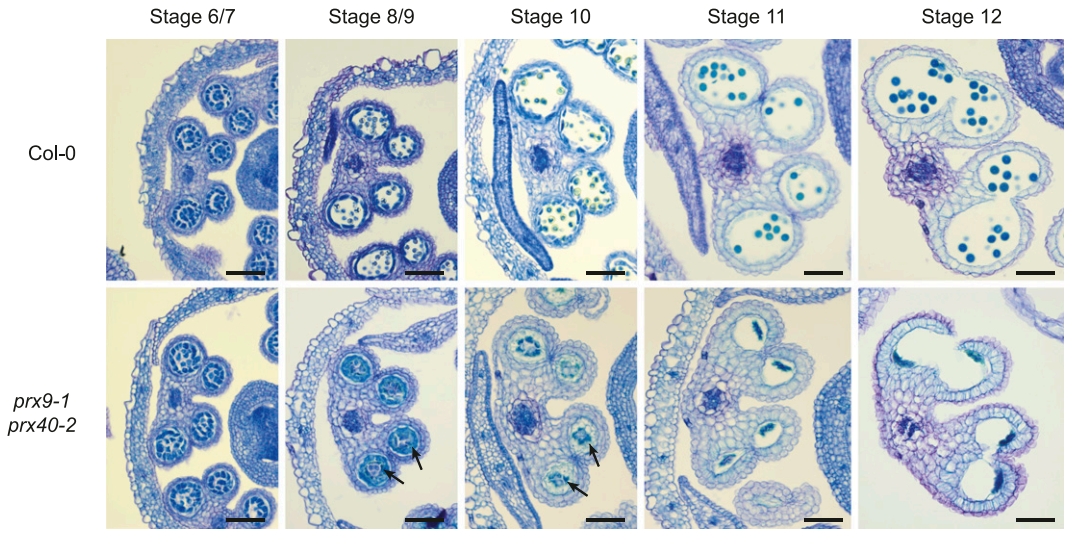

Figure 4. *prx9 prx40* Anthers Display Tapetum Hypertrophy and Pollen Degeneration.

The wild-type (top row) and *prx9-1 prx40-2* (bottom row) anther development from stages 5 to 12 (Sanders et al., 1999). Tapetum swelling in *prx9-1 prx40-2* first appears at stage 8 and persists through stage 10, indicated by arrows. Tapetum PCD and anther dehiscence occur normally in both the wild type and *prx9-1 prx40-2* during stages 11 and 12. Bars = 25 μm.

an immunoblot, comparing protein extracts of the stage 10 (Sanders et al., 1999) wild-type and *prx9-1 prx40-2* anthers (Figure 6C). The wild-type anthers accumulate a putative monomeric extensin at ~40 kD, with higher molecular weight species also present. The most intense bands appeared to be at ~80 kD, corresponding to the molecular weight of an extensin dimer. Additional bands at ~160 and 240 kD were visible, likely corresponding to the molecular weight of a 4-mer and 6-mer, respectively. By comparison, *prx9-1 prx40-2* anthers accumulated substantially less 80-kD extensins and the 160- and 240-kD bands

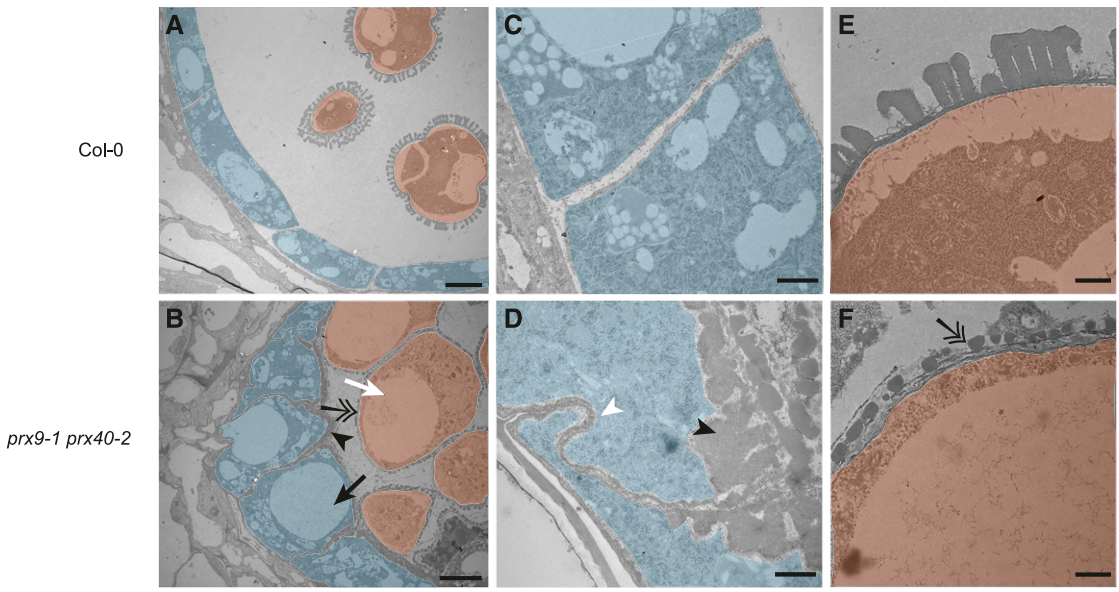

Figure 5. Stage 9 *prx9-1 prx40-2* Anthers Contain Swollen, Hypervacuolated Tapetal Cells and Pollen Grains.

(A) to **(F)** The stage 9 wild-type **(A)** and *prx9-1 prx40-2* **(B)** locules were compared by transmission electron microscopy. Tapetal cells are false colored in blue and developing pollen grains are false colored in orange. The *prx9-1 prx40-2* tapetum is swollen and hypervacuolated (black arrow). Pollen grains are also swollen and hypervacuolated (white arrow). Electron-dense sporopollenin-like material accumulates on the locular face of the tapetum (black arrowhead). Bars = 4 μm. The wild-type tapetal cells **(C)** have rectangular boundaries. *prx9-1 prx40-2* tapetal cells **(D)** have irregular, jigsaw-shaped boundaries (white arrowhead). Bars = 600 nm. The wild-type pollen grains **(E)** have a fully developed exine, whereas *prx9-1 prx40-2* pollen grains **(F)** only have visible probaculae and nexine (double arrow). Bars = 600 nm.

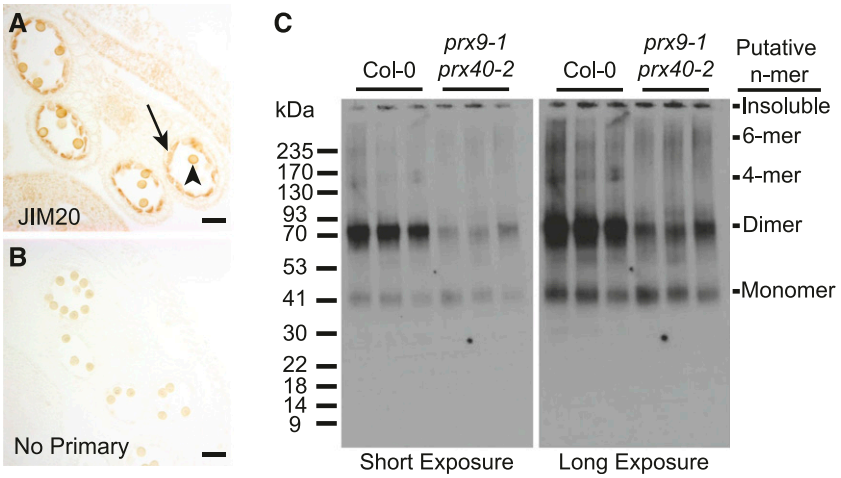

Figure 6. High Molecular Weight JIM20 Extensin Epitopes Accumulate in the Wild-Type, but Not *prx9-1 prx40-2*, Tapetal Cells.

(A) to **(C)** Extensins in the wild-type stage 10 anthers were examined by immunostaining with the JIM20 antibody **(A)** and compared with a control without a primary antibody **(B)**. Staining was most obvious in the tapetum (black arrow) and may also be present in the pollen grain wall (black arrowhead). The apparent molecular weight of extensins was compared between three biological replicates of the wild-type and *prx9-1 prx40-2* stages 10 to 12 (Sanders et al., 1999) anthers by immunoblot **(C)**. Left panel is a short exposure and right panel is a long exposure of the same blot. Similar amounts of a putative ~40-kD monomer are present in both samples. Substantially more putative ~80-kD dimer is present in the wild-type anthers. Higher molecular weight species of ~160 and 240 kD, corresponding to putative 4-mer and 6-mer, respectively, are present in the wild-type anthers but absent from *prx9-1 prx40-2* anthers.

were absent, even though *prx9-1 prx40-2* anthers accumulated approximately the same amount of the putative monomeric species.

If PRX9 and PRX40 are truly extensin peroxidases, they would be sufficient to cross-link a model extensin in a reconstituted system. Because extensins produced in plant cells undergo extensive glycosylation prior to polymerization (Showalter and Basu, 2016), soluble extensins could not be produced in microbial hosts, making in vitro biochemical assays with physiologically relevant monomeric extension substrates intractable. As an alternative

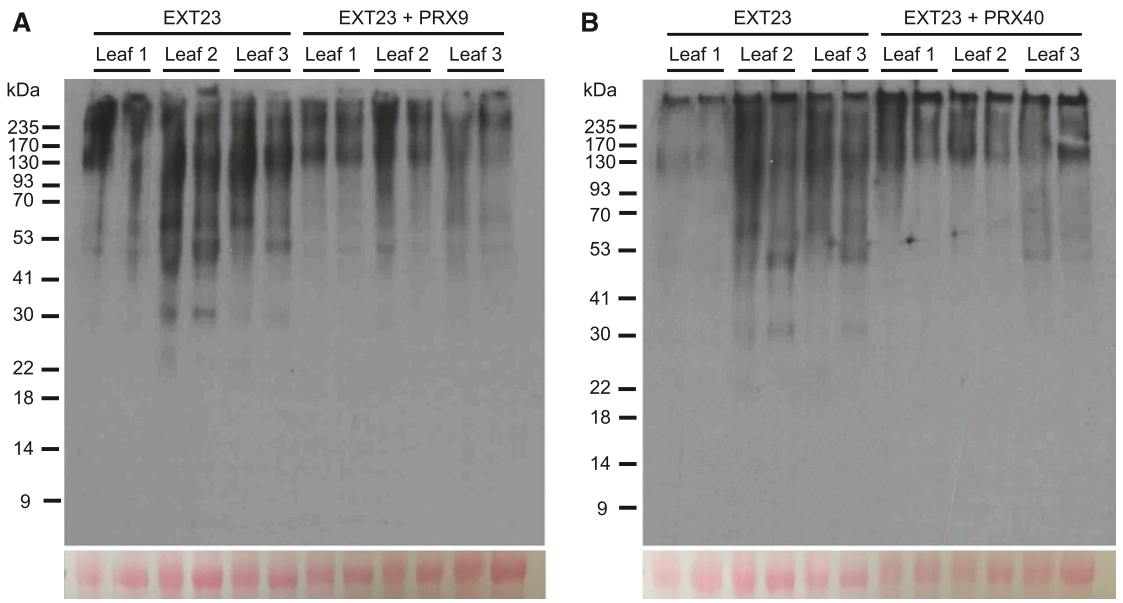

Figure 7. High Molecular Weight Extensins Accumulate in *N. benthamiana* Leaves When Coexpressed with either PRX9 or PRX40.

EXT23 was transiently expressed in *N. benthamiana* leaves, either with or without a peroxidase, and the apparent molecular weights of extensins were analyzed by immunoblotting with JIM20. In each blot, lanes 1 to 6 analyze samples from three independent leaves expressing EXT23. Two independent sample were analyzed from each leaf. Lanes 7 to 12 analyze samples from three independently transformed leaves coexpressing EXT23 with either PRX9 **(A)** or PRX40 **(B)**. The Ponceau-stained Rubisco band is included below each blot to indicate total protein loaded.

approach to test whether PRX9 and PRX40 are capable of cross-linking extensins, we transiently expressed *EXTENSIN23* (*EXT23* [AT5G19810]) in *Nicotiana benthamiana* leaves with or without peroxidase and examined the size distribution of JIM20 extensin epitopes by immunoblot (Figure 7). We chose *EXT23* because it has been shown to be expressed in the anthers (Hruz et al., 2008), and its molecular weight after glycosylation would be roughly equal to the putative extensin monomer that we observed in anther extracts (Figure 6). Overall, we observed that higher molecular weight JIM20 epitopes accumulated in *N. benthamiana* leaves coexpressing either PRX9 (Figure 7A) or PRX40 (Figure 7B) than in those expressing EXT23 alone. Altogether, these data further support the biochemical function of PRX9 and PRX40 as extensin cross-linking peroxidases in planta.

The *ext18* Mutant Partially Phenocopies *prx9 prx40* Anthers

If extensin cross-linking by PRX9 and PRX40 is important for maintaining tapetum and microspore cell size, knockout mutants of the extensins that are substrates for these peroxidases should phenocopy the *prx9 prx40* plants. *EXT18* knockouts have previously been reported to cause defects in male fertility (Choudhary et al., 2015). The *ext18* mutant was reported to exhibit decreased pollen viability, suggesting that EXT18 is likely expressed in the developing anther and may be cross-linked by PRX9 and PRX40. To assess the role of *EXT18* in tapetum development, we performed a histological comparison between *ext18* (genetrap 8324) and the Landsberg erecta-0 wild-type anther development (Figure 8). As previously reported, we observed degenerated pollen grains at later stages of anther development, but no differences in the shape or size of the tapetum at earlier developmental stages. As with EXT23, we observed a shift toward higher molecular weights when EXT18 was coexpressed with either PRX9 or PRX40 in *N. benthamiana* (Supplemental Figure 4). Since we did not observe tapetum hypertrophy in *ext18* plants, additional extensins likely serve as redundant or more prominent substrates for PRX9 and PRX40 in the tapetum.

PRX9 and PRX40 Are Evolutionarily Conserved Class III Peroxidases in Land Plants

Since PRX9 and PRX40 play an essential role in Arabidopsis anther development, we sought to predict whether orthologs are likely to be important in other plant species. To examine the evolution of PRX9 and PRX40, we performed comprehensive phylogenetic analyses of class III peroxidases across diverse land plant lineages. First, we performed a large-scale neighbor-joining phylogenetic analysis using 887 class III peroxidases collected from several reference model plants representing major land plant lineages (Supplemental Figure 5; Supplemental Data Set 1). This initial analysis identified six major phylogenetic clades of peroxidases, termed clades i through vi, that overall agree well with previously published phylogenies (Tognolli et al., 2002). By mapping known functions associated with class III peroxidases to the tree, we observed that the phylogeny does not separate peroxidases by function. For example, lignin peroxidases do not cluster into one unique clade but rather are distributed across clades i, iii, and vi. This reflects the well-recognized substrate promiscuity of class III peroxidases (Shigeto and Tsutsumi, 2016). Under low selective pressure to maintain substrate specificity, lignin peroxidase activities might have evolved multiple times in parallel during land plant evolution

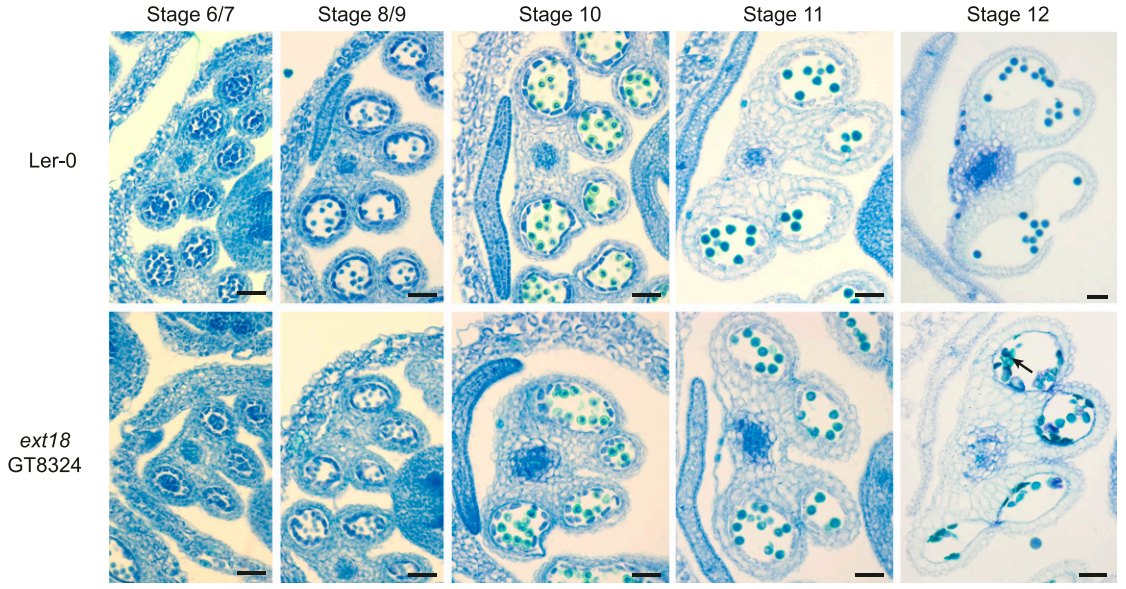

Figure 8. *ext18* Anthers Exhibit Pollen Degeneration, but Not Tapetum Hypertrophy.

The wild-type Landsberg erecta-0 (top row) and *ext18* (bottom row) anther development from stages 5 to 12 (Sanders et al., 1999). The wild-type and *ext18* are indistinguishable until stage 12 when numerous degenerated pollen grains are observed in *ext18* anthers (black arrow). Bars = 25 μm.

through gene duplication followed by neofunctionalization or subfunctionalization.

To gain insight into the deep evolutionary history of *PRX9* and *PRX40*, we then performed a more focused maximum-likelihood phylogenetic analysis using only the sequences from clade i, which contains both *PRX9* and *PRX40* (Figure 9; Supplemental Data Set 2). This analysis revealed that *PRX40* is highly conserved among all major lineages of land plants, with putative orthologs found in species that span bryophytes to angiosperms. By contrast, *PRX9* falls into a smaller clade of orthologs that contains only angiosperm sequences and likely arose by gene duplication. These results suggest that *PRX40* orthologs likely emerged in the common ancestor of all land plants during early land colonization 450 million years ago, whereas *PRX9* emerged through parallel evolution much later within angiosperms.

DISCUSSION

PRX9 and *PRX40* Function to Maintain Tapetum and Microspore Cell Wall Integrity during Anther Development

One of the most defining features of the *prx9 prx40* phenotype is tapetum hypertrophy and subsequent male sterility. Tapetum hypertrophy is a defect in anther development that has been observed in many different contexts across multiple plant species. To our knowledge, tapetum hypertrophy was first reported in rice (*Oryza sativa*) as a stress response to cold (Satake and Hayase, 1970; Mamun et al., 2006) and was later observed in cytoplasmic male-sterile *Capsicum annuum* and in heat- or abscisic acid–treated *Triticum aestivum* (Horner and Rogers, 1974; Saini et al., 1984). These early studies established a connection between

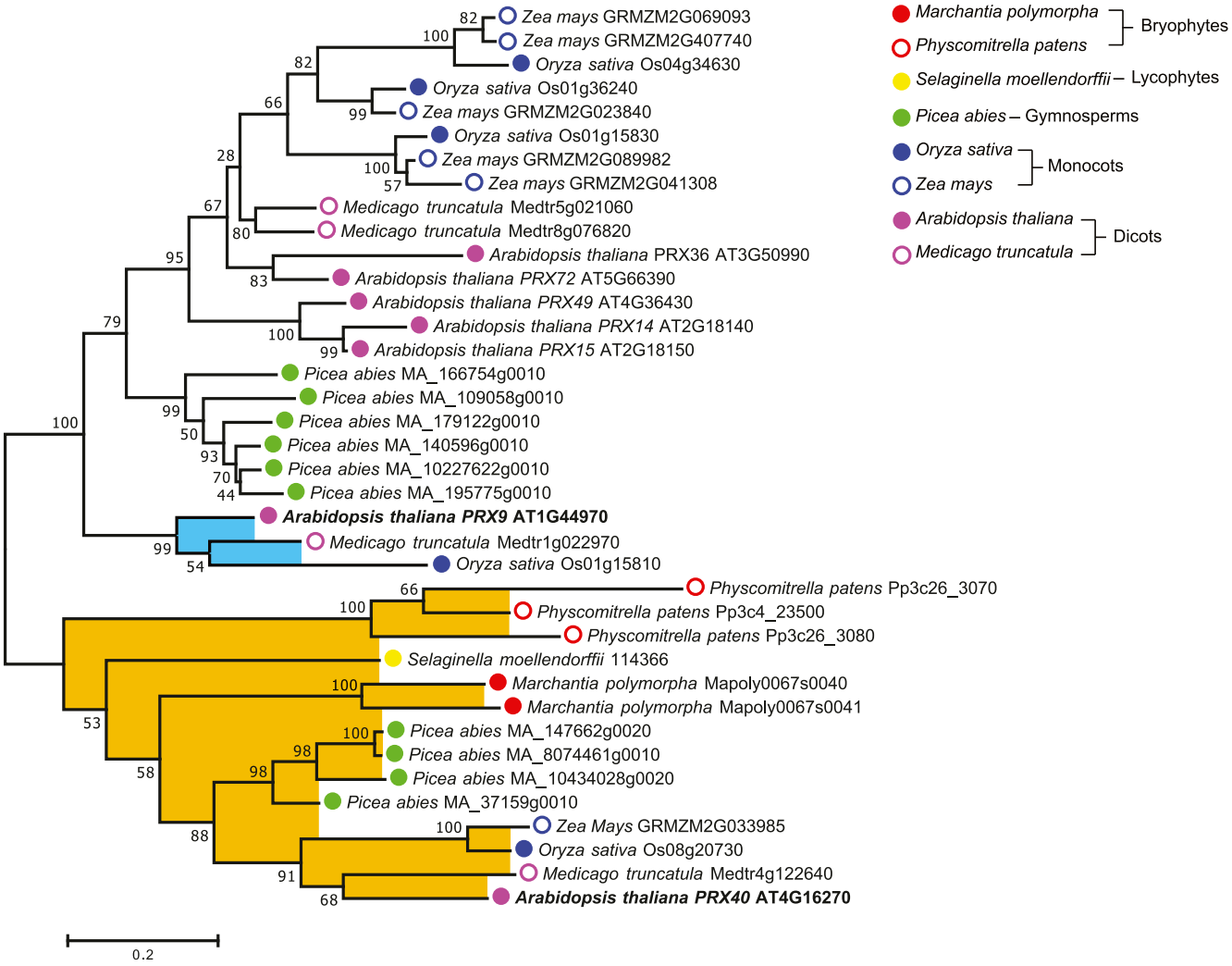

Figure 9. Maximum-Likelihood Phylogenetic Analysis of *PRX9*, *PRX40*, and Related Class III Peroxidases from Various Plant Lineages.

The analysis was generated with 1000 bootstrap replications using a subset of sequences from clade i (Supplemental Figure 4). Bootstrap values are indicated at nodes within the tree. The scale measures evolutionary distance in substitutions per amino acid. *PRX9* is placed within a clade containing only angiosperm sequences, highlighted in blue. *PRX40* is placed in a clade containing sequences spanning land plants from angiosperms to bryophytes, highlighted in orange. *PRX9* and *PRX40* branch labels are bolded.

environmental stress and tapetum hypertrophy–associated male sterility; however, the mechanistic basis for this phenomenon has remained elusive.

In the model plant Arabidopsis, tapetum hypertrophy has not been seen as a stress phenotype but instead was reported as a developmental phenotype associated with a wide collection of mutants, including *roxy1*, *roxy2*, *aborted microspores*, *male sterility1*, *defective in tapetal development and function1*, *dysfunctional tapetum1*, *myb33*, *myb65*, *bhlh010*, *bhlh089*, *bhlh091*, *kaonashi4/uneven pattern of exine1*, *gus negative1*, *gus negative4*, and *fat tapetum* (Sanders et al., 1999; Wilson et al., 2001; Sorensen et al., 2002, 2003; Millar and Gubler, 2005; Zhang et al., 2006; Xing and Zachgo, 2008; Zhu et al., 2008, 2015; Phan et al., 2011; Suzuki et al., 2017). Besides KAONASHI4/UNEVEN PATTERN OF EXINE1, which is a glycosyl transferase, these genes encode regulatory genes and transcription factors or are unmapped mutant alleles. Hence, these mutants provided little insight into a mechanistic understanding of tapetum hypertrophy or how it is prevented in the course of normal anther development in Arabidopsis. *PRX9* and *PRX40* are likely downstream of these transcriptional regulators and directly influence tapetum size by cross-linking extensins in the cell wall.

PRX9 and PRX40 Are Likely Extensin Peroxidases

Extensins are a large family of highly repetitive Hyp-rich glycoproteins that are ubiquitous structural cell wall proteins in land plants (Lamport et al., 2011). Extensins contain alternating hydrophilic and hydrophobic stretches that allow them to self-assemble into dendritic networks (Cannon et al., 2008). The characteristic hydrophilic extensin motif consists of heavily glycosylated Ser-$(Hyp)_{3-5}$ interspersed with hydrophobic Tyr-Val-Tyr (Lamport et al., 2011). Class III peroxidases act on these Tyr residues to form intra- and intermolecular cross-links of extensins.

The tapetal and microspore swelling phenotype seen in *prx9 prx40* anthers is reminiscent of other extensin-associated phenotypes. The best-studied extensin in Arabidopsis is *EXT3/ROOT-SHOOT-HYPOCOTYL-DEFECTIVE* (*RSH*; Hall and Cannon, 2002). Similar to *prx9 prx40* mutants, *rsh* mutants display defects in cell size and shape due to compromised cell walls. Cells within the developing embryos of *rsh* plants are disorganized and fail to form the characteristic heart shape (Hall and Cannon, 2002). Cells throughout seedling roots are also abnormally shaped and dysfunctional. Similarly, mutations in genes involved in extensin glycosylation display phenotypes associated with uninhibited cell expansion, including abnormally elongated roots and petioles, larger rosette leaves, and defects in root hair growth (Gille et al., 2009; Velasquez et al., 2011; Saito et al., 2014; Møller et al., 2017).

Our experimental data also indicate that PRX9 and PRX40 play a role in regulating tapetum and microspore size and shape primarily by their extensin cross-linking activities. We observed the accumulation of extensins in the developing tapetum by immunostaining. Furthermore, we observed that *prx9 prx40* anthers failed to accumulate high molecular weight extensins, a direct consequence of extensin cross-linking in vivo. We also observed that coexpression of either *PRX9* or *PRX40* with EXT23 in *N. benthamiana* leaves resulted in the accumulation of higher molecular weight extensins. Finally, the pollen degeneration seen in *ext18* plants partially phenocopied the *prx9-1 prx40-1* phenotype.

Additionally, previous work has suggested that extensin disassembly is important for tapetal PCD. A papain-like Cys protease, *CYSTEINE ENDOPEPTIDASE1* (*CEP1*), was previously found to be specifically expressed in the tapetum (Zhang et al., 2014). Papain-like Cys proteases have the unique ability to degrade extensins during plant PCD (Helm et al., 2008). Indeed, the Arabidopsis *cep1* mutant displays delayed tapetal PCD, which may be partially explained by its inability to dismantle the extensin scaffold in the tapetum cell wall during late stages of anther development. Altogether, this evidence points to an important role for extensins in the tapetum and microspore cell walls.

PRX9 and PRX40 Substrates: Extensins and H_2O_2

Although EXT18 appears to be a substrate for PRX9 and PRX40, additional extensins are likely involved in the tapetum and microspore cell walls. *EXT23* is expressed in the anthers and appears to be a substrate for transiently expressed *PRX9* and *PRX40* in *N. benthamiana* leaves. Additionally, three extensins or extensin-like genes were found to be upregulated in *cep1* flower buds (Zhang et al., 2014), implying their role in the tapetum: *EXT3/RSH* (AT1G21310), AT5G25550, and *EXT21* (AT2G43150). Of these three, only EXT3 and EXT21 contain the necessary Tyr residues for cross-linking and are therefore possible candidate substrates for PRX9 and PRX40. In addition to *EXT18* (AT1G26250), *EXT19* (AT1G26240) encodes another candidate extensin substrate. *EXT19* is a tandem duplicate of *EXT18* and the two share 84% sequence similarity at the amino acid level. *EXT18* and *EXT19* are arranged head to head in the genome, suggesting that they may be coregulated by a bidirectional promoter. The roles for these extensins in tapetal and pollen walls are likely redundant or partially overlapping. Future work is necessary to dissect the functions of individual extensins and the coordination of these extensions during anther development.

As a cosubstrate for class III peroxidases, H_2O_2 is required for the catalytic function of PRX9 and PRX40. H_2O_2 may be derived from multiple sources in planta. During plant defense and lignification, H_2O_2 is primarily derived from the reduction of molecular oxygen by the respiratory burst oxidase homologs (RBOHs) to superoxide (Marino et al., 2012; Lee et al., 2013) that is further converted to H_2O_2 by superoxide dismutase (SOD). The Arabidopsis genome encodes 10 *RBOHs*: *RBOHA* through *RBOHJ. RBOHE* was shown to be specifically expressed in the tapetum during anther development (Xie et al., 2014). Interestingly, the *rbohe* mutant also displays a mildly hypertrophic tapetum, degenerated pollen grains, and pollen grains with distorted morphologies. Synergistic effects in *rbohe rbohc/rhd2* suggest that *RBOHC* may also play a role in generating tapetal H_2O_2. These phenotypes are consistent with *RBOHE* and *RBOHC* acting upstream of *PRX9* and *PRX40* by generating the superoxide that is subsequently converted to H_2O_2 by a putative SOD. At present, no tapetal *SOD* has been identified or characterized.

In summary, this work identifies *PRX9* and *PRX40* as critical genes for Arabidopsis anther development, likely through their extensin cross-linking activity. *PRX40* is highly conserved among all land plants, suggesting that extensin cross-linking was an

ancient and critical function for the colonization of land by early land plants. *PRX9* likely arose later within angiosperms and descended from a duplication event that can be traced back to a *PRX40* progenitor. At present, most of the 73 class III peroxidases in Arabidopsis have no assigned functions. Future studies may identify additional class III peroxidases as being involved in extensin cross-linking during other developmental processes in plants. Finally, this work sheds light on the mechanism of tapetum hypertrophy, a stress phenotype associated with reductions in crop yield of rice and wheat (*Triticum aestivum*; Satake and Hayase, 1970; Horner and Rogers, 1974; Saini et al., 1984; Mamun et al., 2006). As we continue to expand our understanding of the dynamic signaling and metabolic processes during anther development, we hope to improve our ability to develop stress-resistant crops.

METHODS

Plant Growth Conditions

Arabidopsis (*Arabidopsis thaliana*) Col-0 seeds were placed on water-saturated 3:1 soil:vermiculite supplemented with Osmocote (Greenhouse Megastore). Plants were grown under a 16-h-light/8-h-dark cycle with fluorescent light of 80 to 120 μmol photons m^{-2} s^{-1} at 22°C and 60% RH. T-DNA insertion lines were obtained from the Arabidopsis Biological Resource Center or the Cold Spring Harbor Laboratory and grown under the same conditions.

RT-PCR

Total RNA was extracted from ~100 mg of fresh plant tissue with the RNeasy mini kit (Qiagen) and subjected to an on-column DNase digest to remove contaminating genomic DNA. cDNA was prepared using the SuperScript III Reverse Transcriptase kit (Invitrogen) and used as template for RT-PCR.

GUS Localization

The 507-bp *PRX9* promoter region and 959-bp *PRX40* promoter region were amplified out of Col-0 genomic DNA and ligated into *Bam*HI-linearized pBI101.2 (Gibson Assembly). Assemblies were confirmed by DNA restriction digest and Sanger sequencing and were transformed into *Agrobacterium tumefaciens* GV3101 strain. *Agrobacterium*-mediated Arabidopsis transformation was performed using the floral dip method (Clough and Bent, 1998). T1 kanamycin-resistant transformants were selected on Murashige and Skoog/agar media containing 200 μg/mL Timentin (ticarcillin-clavulanate, Gold Bio) and 50 μg/mL kanamycin. After selection, kanamycin-resistant seedlings were transferred to soil and grown under greenhouse conditions.

For GUS staining, flower buds from adult plants were collected into ice-cold 90% (v/v) acetone and incubated for 20 min at room temperature. Samples were washed in staining buffer (50 mM sodium phosphate, pH 7.2, 0.2% (v/v) Triton X-100, and either 2 or 10 mM potassium ferrocyanide/potassium ferricyanide) and then incubated in staining solution (staining buffer containing 2 mM 5-Bromo-4-chloro-3-indolyl-β-D-glucuronide) on ice. Sample were infiltrated with staining solution under vacuum for 20 min, or until samples sank, and then incubated overnight at 37°C to allow the GUS staining reaction to proceed. The following day, samples were processed through a graded series into 50% (v/v) ethanol and placed in formalin-aceto-alcohol (50% (v/v) ethanol, 10% (v/v) glacial acetic acid, and 5% (w/v) formaldehyde) for fixation. Finally, samples were placed in 70% (v/v) ethanol for examination.

Genotyping

Approximately 1 mg of plant tissue was placed in 50 μL of Tris-EDTA buffer (10 mM Tris, pH 8, and 1 mM EDTA). Tissue was ground with a pestle, and 1 μL of the crude extract was used as a template for genotyping PCR. Genotyping primers were designed using the SIGnal Salk T-DNA primer design tool (http://signal.salk.edu/tdnaprimers.2.html; Supplemental Table).

Paraffin Histology and Histochemistry

Formalin-aceto-alcohol–fixed flower buds were transferred through a graded series into 100% ethanol and then through a graded series into 100% *tert*-butanol. Samples were then processed to paraplast and embedded in paraffin wax blocks. Then, 8- to 10-μm sections were collected with a microtome, transferred to slides, and dried overnight at 37°C. For GUS-stained samples, slides were deparaffinized with two changes of Histo-Clear (National Diagnostics) and cover slipped with Permount (Thermo Fisher Scientific). For toluidine blue staining, samples were deparaffinized with Histo-Clear, rehydrated, stained with 0.5% toluidine blue, dehydrated, and cover slipped with Permount.

Scanning Electron Microscopy

Pollen grains were collected from open flowers and transferred to carbon adhesive tabs (Electron Microscopy Sciences) that were placed on aluminum mounts (Electron Microscopy Sciences). Samples were sputter coated with Au/Pd with a Hummer sputter coater and imaged with JEOL 5600 LV scanning electron microscope. For scanning electron microscopy of anthers, samples were fixed in 2% glutaraldehyde, 3% paraformaldehyde, 0.1 M sodium cacodylate, pH 7.4, 5% Suc, and 0.01% Triton X-100 overnight. Fixed samples were dehydrated through a graded series into 100% ethanol, critical point dried in a critical point dryer (Tousimis), and sputter coated.

Transmission Electron Microscopy

Stage 12 flower buds were fixed in 2.5% glutaraldehyde and 3% paraformaldehyde with 5% Suc in 0.1 M sodium cacodylate buffer, pH 7.4, and 0.01% Triton X-100 overnight. Samples were postfixed in 1% OsO_4 in veronal-acetate buffer. Samples were stained en block overnight with 0.5% uranyl acetate in veronal-acetate buffer, pH 6.0, dehydrated, and embedded in Embed-812 resin. Sections were cut on a Leica EM UC7 ultramicrotome with a Diatome diamond knife at a thickness setting of 50 nm and stained with 2% uranyl acetate and lead citrate. The sections were examined using a Field Electron and Ion Company Tecnai spirit at 80 kV and photographed with an AMT charge-coupled device camera.

Immunostaining

Ten-micrometer sections were collected from paraffin-embedded flower buds, deparaffinized with Histo-Clear, and transferred into water through a graded series of ethanol. Sections were equilibrated in PBS and then blocked with 3% dry nonfat milk. Next, 10 μL of undiluted JIM20 hybridoma supernatant (CarboSource) was added to the sections and incubated overnight at 4°C. Primary antibody was washed away with five exchanges of PBS and 10 μL of 1:10,000 mouse anti-rat IgM secondary antibody-horseradish peroxidase (catalog no. 31,476; Thermo Fisher Scientific) was added to sections and incubated at room temperature for 1 h. Secondary antibody was washed away with five exchanges of PBS. Next, 20 μL of 0.05% diaminobenzidine/0.015% H_2O_2 was added and allowed to incubate until sections showed robust staining. Reactions were stopped with a rapid dilution into MilliQ water and four subsequent exchanges with fresh MilliQ water.

Immunoblotting

Stages 10 to 12 anthers were dissected out of individual flower buds, frozen on dry ice, and ground in a microcentrifuge tube with a pestle. Next, 50 μL of extraction buffer (25 mM Tris, pH 8, and 4% SDS) was added, and the samples were mixed thoroughly with the pestle. Extracts were refrozen and stored at −20°C. Ten-microliter samples were separated on 3-(*N*-morpholino)-propanesulfonic acid-Tris SDS-PAGE gels and transferred to nitrocellulose membranes. Membranes were blocked with 5% dry non-fat milk in Tris-buffered saline-Tween and incubated with 1:50 JIM20 overnight at 4°C. Membranes were washed five times with Tris-buffered saline-Tween and incubated with 1:10,000 mouse anti-rat IgM secondary antibody-horseradish peroxidase (Thermo Fisher Scientific). Immunostaining was visualized with the Enhance Chemiluminescence kit (Thermo Fisher Scientific).

Heterologous Protein Expression in *Nicotiana benthamiana*

Agrobacterium tumefaciens LBA4404 was transformed with pEAQ-HT vector constructs by electroporation (2.5 kV) and plated on yeast and mold (YM) agar (0.4 g of yeast extract, 10 g of mannitol, 0.1 g of sodium chloride, 0.2 g of magnesium sulfate [heptahydrate], 0.5 g of potassium phosphate [dibasic, trihydrate], 15 g of agar, and 1 L of MilliQ water, pH 7) with 100 μg/mL rifampicin, 50 μg/mL kanamycin, and 100 μg/mL streptomycin, and incubated for 2 d at 30°C. A 5-mL starter culture of YM medium with 100 μg/mL rifampicin, 50 μg/mL kanamycin, and 100 μg/mL streptomycin was inoculated with a clone of *Agrobacterium tumefaciens* LBA4404 containing the plasmid and incubated for 24 to 36 h at 30°C/225 rpm. The starter culture was used to inoculate a 35-mL culture of YM medium with 100 μg/mL rifampicin, 50 μg/mL kanamycin, and 100 μg/mL streptomycin, which was incubated for 24 h at 30°C/225 rpm. The 35-mL cultures were pelleted by centrifugation for 15 min at 5000 rpm at 4°C, the supernatant was discarded, and the cells were resuspended in PBS to give a final OD of 0.8. The *Agrobacterium* suspensions were syringe infiltrated into *N. benthamiana*, and the plants were placed in shade overnight. Infiltrated *Nicotiana* plants were grown in greenhouse conditions for 5 d before tissue was harvested and analyzed by immunoblot.

Recombinant Protein Expression and Refolding Optimization

PRX9 and *PRX40* coding sequences were cloned without their predicted signal peptide sequences into the pHIS8-4 bacterial expression vector with an N-terminal His-tag and transformed into *Escherichia coli* BL-21(DE3). Next, 500 mL of transformed bacteria were grown in Terrific broth at 37°C/225 rpm until reaching an OD_{600} of 0.8. Cultures were induced with 500 μM isopropyl β-D-thiogalactoside and incubated overnight at 16°C/225 rpm. Cultures were pelleted by centrifugation for 15 min at 6000 rpm/4°C, and pellets were resuspended in 12 mL of lysis buffer (50 mM Tris, pH 8, 500 mM NaCl, and 30 mM imidazole). Resuspensions were divided into 1-mL aliquots, frozen, and stored at −80°C.

Resuspensions were thawed and lysed by sonication for 20 s. Lysates were centrifuged for 30 min at 16,000 rpm/4°C, and supernatants were discarded. Insoluble PRX9 and PRX40 were washed three times by resuspending the pellets in lysis buffer with 2 M urea, spinning for 30 min at 16,000 rpm/4°C, and discarding the supernatant. PRX9 and PRX40 were then solubilized in lysis buffer with 8 M urea and bound to nickel-nitrilotriacetic acid resin to separate them from bacterial cell material. Protein-bound nickel-nitrilotriacetic resin was diluted into elution buffer (50 mM Tris, pH 8, 500 mM NaCl, and 300 mM imidazole) with 8 M urea, and the resin was separated from the elution by centrifugation for 10 min at 10,000 rpm/4°C.

Refolding conditions were tested by diluting 10 μL of HisTrap elution into 190 μL of various refolding conditions in a 96-well plate format. All wells contained 10 mM MES, pH 6, 5 mM $CaCl_2$, 5 μM hemin, and 0.7 mM GSSG. Concentrations of urea and GSH were varied. Wells were sealed with an adhesive plate cover, and the plate was incubated for 60 h in darkness at room temperature. Next, 50 μL of refolding reactions was added to 50 μL of pyrogallol reaction buffer (final concentration: 10 mM MES, pH 6, 50 mM pyrogallol, and 1 mM H_2O_2). The relative activity of refolding conditions was assessed by monitoring the formation of purpurogallin, which is yellow and absorbs light at 420 nm.

Phylogenetic Analysis

Protein sequences from Arabidopsis, *Medicago truncatula*, *Oryza sativa*, *Zea mays*, *Selaginella moellendorffii*, *Physcomitrella patens*, and *Marchantia polymorpha* genomes were collected from Phytozome (https://phytozome.jgi.doe.gov) by BLAST search. *Picea abies* sequences were collected by BLAST search from Congenie (http://congenie.org/). Incomplete sequences were manually excluded by eye, and sequences were aligned in MEGA6 (Tamura et al., 2013) with the MUSCLE algorithm (Edgar, 2004). For the large-scale phylogeny (Supplemental Figure 4), all 877 sequences were included. The tree was generated with the neighbor-joining method (Saitou and Nei, 1987). Evolutionary distances were calculated using the Jones–Taylor–Thornton matrix-based method (Jones et al., 1992) and are in units of number of amino acid substitutions per site.

For the maximum-likelihood tree (Figure 9), only the sequences from clade i of the neighbor-joining tree were included. Sequences were realigned in MEGA6 with MUSCLE. Positions in the alignment that were represented by only a single sequence were manually removed and the truncated sequences were realigned. A distance matrix was generated in MEGA6 and sequences with high divergence from *PRX9* and *PRX40* were manually removed. Several preliminary phylogenies were generated and sequences that could not be confidently placed on branches that related to *PRX9* or *PRX40* were manually removed. The final phylogeny was generated with the remaining sequences using the maximum-likelihood method based on the Whelan and Goldman model (Whelan and Goldman, 2001). A discrete Gamma distribution was used to model evolutionary rate differences among sites (five categories [+G, parameter = 0.7211]). Branch lengths were measured in the number of substitutions per site.

Accession Numbers

Sequence data from this article can be found in the EMBL/GenBank data libraries under accession numbers AT1G44970 (*PRX9*), AT4G16270 (*PRX40*), AT3G18780 (*ACTIN2*), AT5G19810 (*EXT23*), and AT1G26250 (*EXT18*).

Supplemental Data

Supplemental Figure 1. BAR eFP predicts *PRX9* and *PRX40* are expressed in early flower buds.

Supplemental Figure 2. Anther filaments from stage 14 *prx9-1 prx40-2* flower are not fully elongated.

Supplemental Figure 3. Reconstituted enzyme activity can be obtained by solubilizing, purifying, and refolding protein from *E. coli* expressing PRX9 and PRX40.

Supplemental Figure 4. PRX9 and PRX40 cross-link EXT18 when transiently expressed in *Nicotiana benthamiana*.

Supplemental Figure 5. Neighbor-joining phylogenetic analysis of class III peroxidases across land plants.

Supplemental Table. List of primers used in this study.

Supplemental Data Set 1. Alignment of class III peroxidases protein sequences used for large-scale neighbor-joining phylogenetic analysis (Supplemental Figure 5).

Supplemental Data Set 2. Alignment of sequences used for maximum-likelihood analysis (Figure 9).

ACKNOWLEDGMENTS

We thank Nicki Watson at the Whitehead Institute Keck Imaging Facility for assistance with electron microscopy. This work was supported by the Pew Scholars Program in the Biomedical Sciences (27345), the Searle Scholars Program Kinship Foundation (15-SSP-162), and the National Science Foundation (CHE-1709616). J.R.J. was supported by the National Science Foundation Graduate Research Fellowship (1122374).

AUTHOR CONTRIBUTIONS

J.R.J. and J.K.W. designed and analyzed all experiments. J.R.J. and W.C.D. performed the experiments. J.R.J. and J.K.W. wrote the article.

Received November 28, 2018; revised February 6, 2019; accepted March 13, 2019; published March 18, 2019.

REFERENCES

Bernards, M.A., Fleming, W.D., Llewellyn, D.B., Priefer, R., Yang, X., Sabatino, A., and Plourde, G.L. (1999). Biochemical characterization of the suberization-associated anionic peroxidase of potato. Plant Physiol. **121:** 135–146.

Brady, J.D., Sadler, I.H., and Fry, S.C. (1996). Di-isodityrosine, a novel tetrametric derivative of tyrosine in plant cell wall proteins: A new potential cross-link. Biochem. J. **315:** 323–327.

Brownleader, M.D., Ahmed, N., Trevan, M., Chaplin, M.F., and Dey, P.M. (1995). Purification and partial characterization of tomato extensin peroxidase. Plant Physiol. **109:** 1115–1123.

Brownleader, M.D., Hopkins, J., Mobasheri, A., Dey, P.M., Jackson, P., and Trevan, M. (2000). Role of extensin peroxidase in tomato (Lycopersicon esculentum Mill.) seedling growth. Planta **210:** 668–676.

Cannon, M.C., Terneus, K., Hall, Q., Tan, L., Wang, Y., Wegenhart, B.L., Chen, L., Lamport, D.T., Chen, Y., and Kieliszewski, M.J. (2008). Self-assembly of the plant cell wall requires an extensin scaffold. Proc. Natl. Acad. Sci. USA **105:** 2226–2231.

Cecchetti, V., Altamura, M.M., Falasca, G., Costantino, P., and Cardarelli, M. (2008). Auxin regulates Arabidopsis anther dehiscence, pollen maturation, and filament elongation. Plant Cell **20:** 1760–1774.

Choudhary, P., Saha, P., Ray, T., Tang, Y., Yang, D., and Cannon, M.C. (2015). EXTENSIN18 is required for full male fertility as well as normal vegetative growth in Arabidopsis. Front. Plant Sci. **6:** 553.

Clough, S.J., and Bent, A.F. (1998). Floral dip: A simplified method for *Agrobacterium*-mediated transformation of *Arabidopsis thaliana*. Plant J. **16:** 735–743.

Duroux, L., and Welinder, K.G. (2003). The peroxidase gene family in plants: A phylogenetic overview. J. Mol. Evol. **57:** 397–407.

Edgar, R.C. (2004). MUSCLE: Multiple sequence alignment with high accuracy and high throughput. Nucleic Acids Res. **32:** 1792–1797.

Fernández-Marcos, M., Desvoyes, B., Manzano, C., Liberman, L.M., Benfey, P.N., Del Pozo, J.C., and Gutierrez, C. (2017). Control of Arabidopsis lateral root primordium boundaries by MYB36. New Phytol. **213:** 105–112.

Fernández-Pérez, F., Pomar, F., Pedreño, M.A., and Novo-Uzal, E. (2015a). The suppression of AtPrx52 affects fibers but not xylem lignification in Arabidopsis by altering the proportion of syringyl units. Physiol. Plant. **154:** 395–406.

Fernández-Pérez, F., Vivar, T., Pomar, F., Pedreño, M.A., and Novo-Uzal, E. (2015b). Peroxidase 4 is involved in syringyl lignin formation in *Arabidopsis thaliana*. J. Plant Physiol. **175:** 86–94.

Fry, S.C. (1982). Isodityrosine, a new cross-linking amino acid from plant cell-wall glycoprotein. Biochem. J. **204:** 449–455.

Gille, S., Hänsel, U., Ziemann, M., and Pauly, M. (2009). Identification of plant cell wall mutants by means of a forward chemical genetic approach using hydrolases. Proc. Natl. Acad. Sci. USA **106:** 14699–14704.

Hall, Q., and Cannon, M.C. (2002). The cell wall hydroxyproline-rich glycoprotein RSH is essential for normal embryo development in Arabidopsis. Plant Cell **14:** 1161–1172.

Hao, Z., et al. (2014). Loss of Arabidopsis GAUT12/IRX8 causes anther indehiscence and leads to reduced G lignin associated with altered matrix polysaccharide deposition. Front. Plant Sci. **5:** 357.

Helm, M., Schmid, M., Hierl, G., Terneus, K., Tan, L., Lottspeich, F., Kieliszewski, M.J., and Gietl, C. (2008). KDEL-tailed cysteine endopeptidases involved in programmed cell death, intercalation of new cells, and dismantling of extensin scaffolds. Am. J. Bot. **95:** 1049–1062.

Herrero, J., Fernández-Pérez, F., Yebra, T., Novo-Uzal, E., Pomar, F., Pedreño, M.Á., Cuello, J., Guéra, A., Esteban-Carrasco, A., and Zapata, J.M. (2013). Bioinformatic and functional characterization of the basic peroxidase 72 from *Arabidopsis thaliana* involved in lignin biosynthesis. Planta **237:** 1599–1612.

Heslop-Harrison, J. (1968). Pollen wall development. The succession of events in the growth of intricately patterned pollen walls is described and discussed. Science **161:** 230–237.

Horner, H.T., Jr., and Rogers, M.A. (1974). A comparative light and electron microscopic study of microsporogenesis in male-fertile and cytoplasmic male-sterile pepper (*Capsicum annuum*). Can. J. Bot. **52:** 435–441.

Hruz, T., Laule, O., Szabo, G., Wessendorp, F., Bleuler, S., Oertle, L., Widmayer, P., Gruissem, W., and Zimmermann, P. (2008). Genevestigator v3: A reference expression database for the meta-analysis of transcriptomes. Adv. Bioinforma. **2008:** 420747.

Jackson, P.A., Galinha, C.I., Pereira, C.S., Fortunato, A., Soares, N.C., Amâncio, S.B., and Pinto Ricardo, C.P. (2001). Rapid deposition of extensin during the elicitation of grapevine callus cultures is specifically catalyzed by a 40-kilodalton peroxidase. Plant Physiol. **127:** 1065–1076.

Jones, D.T., Taylor, W.R., and Thornton, J.M. (1992). The rapid generation of mutation data matrices from protein sequences. Comput. Appl. Biosci. **8:** 275–282.

Knox, R.B., Heslop-Harrison, J., and Reed, C. (1970). Localization of antigens associated with the pollen grain wall by immunofluorescence. Nature **225:** 1066–1068.

Kunieda, T., Shimada, T., Kondo, M., Nishimura, M., Nishitani, K., and Hara-Nishimura, I. (2013). Spatiotemporal secretion of PEROXIDASE36 is required for seed coat mucilage extrusion in Arabidopsis. Plant Cell **25:** 1355–1367.

Lamport, D.T.A., Kieliszewski, M.J., Chen, Y., and Cannon, M.C. (2011). Role of the extensin superfamily in primary cell wall architecture. Plant Physiol. **156:** 11–19.

Lee, Y., Rubio, M.C., Alassimone, J., and Geldner, N. (2013). A mechanism for localized lignin deposition in the endodermis. Cell **153:** 402–412.

Li, D.-D., Xue, J.-S., Zhu, J., and Yang, Z.-N. (2017). Gene regulatory network for tapetum development in *Arabidopsis thaliana.* Front. Plant Sci. **8:** 1559.

Liszkay, A., van der Zalm, E., and Schopfer, P. (2004). Production of reactive oxygen intermediates (O(2)(.-), H(2)O(2), and (.)OH) by maize roots and their role in wall loosening and elongation growth. Plant Physiol. **136:** 3114–3123, discussion 3001.

Mamun, E.A., Alfred, S., Cantrill, L.C., Overall, R.L., and Sutton, B.G. (2006). Effects of chilling on male gametophyte development in rice. Cell Biol. Int. **30:** 583–591.

Marino, D., Dunand, C., Puppo, A., and Pauly, N. (2012). A burst of plant NADPH oxidases. Trends Plant Sci. **17:** 9–15.

Millar, A.A., and Gubler, F. (2005). The Arabidopsis GAMYB-like genes, MYB33 and MYB65, are microRNA-regulated genes that redundantly facilitate anther development. Plant Cell **17:** 705–721.

Møller, S.R., et al. (2017). Identification and evolution of a plant cell wall specific glycoprotein glycosyl transferase, ExAD. Sci. Rep. **7:** 45341.

Obayashi, T., Kinoshita, K., Nakai, K., Shibaoka, M., Hayashi, S., Saeki, M., Shibata, D., Saito, K., and Ohta, H. (2007). ATTED-II: a database of co-expressed genes and cis elements for identifying co-regulated gene groups in Arabidopsis. Nucleic Acids Res. **35:** D863–D869.

Pattathil, S., et al. (2010). A comprehensive toolkit of plant cell wall glycan-directed monoclonal antibodies. Plant Physiol. **153:** 514–525.

Phan, H.A., Iacuone, S., Li, S.F., and Parish, R.W. (2011). The MYB80 transcription factor is required for pollen development and the regulation of tapetal programmed cell death in *Arabidopsis thaliana*. Plant Cell **23:** 2209–2224.

Quilichini, T.D., Grienenberger, E., and Douglas, C.J. (2015). The biosynthesis, composition and assembly of the outer pollen wall: A tough case to crack. Phytochemistry **113:** 170–182.

Ringli, C. (2010). The hydroxyproline-rich glycoprotein domain of the Arabidopsis LRX1 requires Tyr for function but not for insolubilization in the cell wall. Plant J. **63:** 662–669.

Saini, H.S., Sedgley, M., and Aspinall, D. (1984). Development anatomy in wheat of male sterility induced by heat stress, water deficit or abscisic acid. Funct. Plant Biol. **11:** 243–253.

Saito, F., Suyama, A., Oka, T., Yoko-O, T., Matsuoka, K., Jigami, Y., and Shimma, Y.-I. (2014). Identification of novel peptidyl serine α-galactosyltransferase gene family in plants. J. Biol. Chem. **289:** 20405–20420.

Saitou, N., and Nei, M. (1987). The neighbor-joining method: A new method for reconstructing phylogenetic trees. Mol. Biol. Evol. **4:** 406–425.

Sanders, P.M., Bui, A.Q., Weterings, K., McIntire, K.N., Hsu, Y.-C., Lee, P.Y., Truong, M.T., Beals, T.P., and Goldberg, R.B. (1999). Anther developmental defects in *Arabidopsis thaliana* male-sterile mutants. Sex. Plant Reprod. **11:** 297–322.

Satake, T., and Hayase, H. (1970). Male sterility caused by cooling treatment at the young microspore stage in rice plants: V. Estimations of pollen developmental stage and the most sensitive stage to coolness. Jpn. J. Crop. Sci. **39:** 468–473.

Shigeto, J., and Tsutsumi, Y. (2016). Diverse functions and reactions of class III peroxidases. New Phytol. **209:** 1395–1402.

Shigeto, J., Itoh, Y., Hirao, S., Ohira, K., Fujita, K., and Tsutsumi, Y. (2015). Simultaneously disrupting AtPrx2, AtPrx25 and AtPrx71 alters lignin content and structure in Arabidopsis stem. J. Integr. Plant Biol. **57:** 349–356.

Showalter, A.M., and Basu, D. (2016). Extensin and arabinogalactan-protein biosynthesis: glycosyltransferases, research challenges, and biosensors. Front. Plant Sci. **7:** 814.

Smith, A.T., Santama, N., Dacey, S., Edwards, M., Bray, R.C., Thorneley, R.N., and Burke, J.F. (1990). Expression of a synthetic gene for horseradish peroxidase C in *Escherichia coli* and folding and activation of the recombinant enzyme with Ca2+ and heme. J. Biol. Chem. **265:** 13335–13343.

Sorensen, A., Guerineau, F., Canales-Holzeis, C., Dickinson, H.G., and Scott, R.J. (2002). A novel extinction screen in *Arabidopsis thaliana* identifies mutant plants defective in early microsporangial development. Plant J. **29:** 581–594.

Sorensen, A.-M., Kröber, S., Unte, U.S., Huijser, P., Dekker, K., and Saedler, H. (2003). The Arabidopsis ABORTED MICROSPORES (AMS) gene encodes a MYC class transcription factor. Plant J. **33:** 413–423.

Suzuki, T., Narciso, J.O., Zeng, W., van de Meene, A., Yasutomi, M., Takemura, S., Lampugnani, E.R., Doblin, M.S., Bacic, A., and Ishiguro, S. (2017). KNS4/UPEX1: A type II arabinogalactan β-(1,3)-galactosyltransferase required for pollen exine development. Plant Physiol. **173:** 183–205.

Tamura, K., Stecher, G., Peterson, D., Filipski, A., and Kumar, S. (2013). MEGA6: Molecular Evolutionary Genetics Analysis version 6.0. Mol. Biol. Evol. **30:** 2725-2729.

Tognolli, M., Penel, C., Greppin, H., and Simon, P. (2002). Analysis and expression of the class III peroxidase large gene family in *Arabidopsis thaliana*. Gene **288:** 129–138.

Tsukagoshi, H., Busch, W., and Benfey, P.N. (2010). Transcriptional regulation of ROS controls transition from proliferation to differentiation in the root. Cell **143:** 606–616.

Velasquez, S.M., et al. (2011). O-Glycosylated cell wall proteins are essential in root hair growth. Science **332:** 1401–1403.

Waese, J., and Provart, N.J. (2017). The bio-analytic resource for plant biology. Methods Mol. Biol. **1533:** 119–148.

Welinder, K.G., Justesen, A.F., Kjaersgård, I.V., Jensen, R.B., Rasmussen, S.K., Jespersen, H.M., and Duroux, L. (2002). Structural diversity and transcription of class III peroxidases from *Arabidopsis thaliana*. Eur. J. Biochem. **269:** 6063–6081.

Weng, J.-K., and Chapple, C. (2010). The origin and evolution of lignin biosynthesis. New Phytol. **187:** 273–285.

Whelan, S., and Goldman, N. (2001). A general empirical model of protein evolution derived from multiple protein families using a maximum-likelihood approach. Mol. Biol. Evol. **18:** 691–699.

Wilson, Z.A., Morroll, S.M., Dawson, J., Swarup, R., and Tighe, P.J. (2001). The Arabidopsis MALE STERILITY1 (MS1) gene is a transcriptional regulator of male gametogenesis, with homology to the PHD-finger family of transcription factors. Plant J. **28:** 27–39.

Winter, D., Vinegar, B., Nahal, H., Ammar, R., Wilson, G.V., and Provart, N.J. (2007). An "electronic fluorescent pictograph" browser for exploring and analyzing large-scale biological data sets. PLoS One **2:** e718.

Xie, H.-T., Wan, Z.-Y., Li, S., and Zhang, Y. (2014). Spatiotemporal production of reactive oxygen species by NADPH oxidase is critical for tapetal programmed cell death and pollen development in Arabidopsis. Plant Cell **26:** 2007–2023.

Xing, S., and Zachgo, S. (2008). ROXY1 and ROXY2, two Arabidopsis glutaredoxin genes, are required for anther development. Plant J. **53:** 790–801.

Yang, C., Song, J., Ferguson, A.C., Klisch, D., Simpson, K., Mo, R., Taylor, B., Mitsuda, N., and Wilson, Z.A. (2017). Transcription factor MYB26 is key to spatial specificity in anther secondary thickening formation. Plant Physiol. **175:** 333–350.

Zhang, D., Liu, D., Lv, X., Wang, Y., Xun, Z., Liu, Z., Li, F., and Lu, H. (2014). The cysteine protease CEP1, a key executor involved in tapetal programmed cell death, regulates pollen development in Arabidopsis. Plant Cell **26:** 2939–2961.

Zhang, W., Sun, Y., Timofejeva, L., Chen, C., Grossniklaus, U., and Ma, H. (2006). Regulation of Arabidopsis tapetum development and function by DYSFUNCTIONAL TAPETUM1 (DYT1) encoding a putative bHLH transcription factor. Development **133:** 3085–3095.

Zhu, E., You, C., Wang, S., Cui, J., Niu, B., Wang, Y., Qi, J., Ma, H., and Chang, F. (2015). The DYT1-interacting proteins bHLH010, bHLH089 and bHLH091 are redundantly required for Arabidopsis anther development and transcriptome. Plant J. **83:** 976–990.

Zhu, J., Chen, H., Li, H., Gao, J.-F., Jiang, H., Wang, C., Guan, Y.-F., and Yang, Z.-N. (2008). Defective in Tapetal development and function 1 is essential for anther development and tapetal function for microspore maturation in Arabidopsis. Plant J. **55:** 266–277.